TEMPEST-D and GPM-GMI Observations Over Precipitating Systems: A Cross-Validation Study

Chandrasekar Radhakrishnan, V. Chandrasekar, *Fellow, IEEE*, Steven C. Reising, *Senior Member, IEEE*, Wesley Berg, and Shannon T. Brown, *Senior Member, IEEE*

***Abstract*—The objective of this study is to cross-validate observations over precipitating systems by microwave radiometers on the temporal experiment for storms and tropical systems demonstration (TEMPEST-D) CubeSat mission and the global precipitation measurement microwave imager (GMI). The purpose of this article is twofold: first, to show consistency between TEMPEST-D and GMI observations, and second, to demonstrate the potential to enhance temporal sampling when TEMPEST-D and GMI observations are merged. Two cross-validation methodologies were employed. The first cross-validation methodology is to quantitatively compare TEMPEST-D and GMI brightness temperature (TB) observations over precipitation systems using a priori spatiotemporal constraints. The comparative analysis showed that the two instruments' TB observations have similar probability distributions, with a mean absolute difference of 2.9 K. The second cross-validation methodology is to quantitatively compare TEMPEST-D and GMI TB observations over tropical cyclone systems. Three storm cases were analyzed in this comparative study. The analysis showed that the structure and intensity of the storms are similar in TEMPEST-D and GMI TB observations, and the overall average correlation coefficient (*r*) is 0.9. Combining TEMPEST-D and GMI TB observations over the hurricane systems increased the sampling frequency by a factor of 2.5, compared to using the GMI data alone.**

***Index Terms*—Brightness temperature (TB), CubeSat, global microwave imager, global precipitation mission, hurricane, microwave radiometer, temporal experiment for storms and tropical systems demonstration (TEMPEST-D), tropical cyclone, typhoon.**

I. Introduction

THE knowledge of precipitation over land and the world's oceans is essential to understand the development and evolution of oceanic storms, especially cyclonic storms that may make landfall and cause damage to life and property. Weather satellites are a critical part of the infrastructure used to monitor storms over the world's oceans. Passive microwave (PMW) sensors have a long heritage of performing observations over convective storms. Even though PMW sensors have been shown to be very useful, they are currently available only in low Earth orbit (LEO) [1], [2], [3]. Therefore, they have limited temporal resolution compared to visible and Infrared sensors in geostationary orbit satellites as well as ground-based radar observations. High temporal resolution observations on time scales of tens of minutes are needed to monitor the evolution of storms for various applications, including storm tracking and prediction of intensity. Recent use of CubeSat and small satellite technology has provided a viable and cost-effective approach to observe storms and precipitation systems at a reasonable temporal resolution using satellite constellations. Kulu et al. [4] reported that as of August 1, 2022, more than 1897 CubeSats had been successfully deployed in LEO. Goncharenko et al. [5] analyzed CubeSat constellations and demonstrated their capability of reducing average revisit time at a reasonable cost. Observations from new microwave radiometric sensors need to be cross validated and calibrated before ingesting them into operational weather models and combining them with other satellite observations to generate global weather products. A number of studies have been conducted for validation of CubeSat brightness temperature (TB) observations and cross comparison with other satellite observations. Schulte et al. [6] used the Colorado State University one-dimensional variational retrieval algorithm to retrieve total precipitable water, cloud liquid water path, and cloud ice water path from the temporal experiment for storms and tropical systems demonstration (TEMPEST-D) and microwave humidity sounder (MHS) observations. The retrievals showed that TEMPEST-D has similar performance to the larger MHS on traditional MetOp satellites. Validation of TEMPEST-D observations through cross calibration with scientific and operational satellite sensors [7] showed that even though TEMPEST-D is a 6U CubeSat (20 cm × 10 cm × 34 cm dimensions), it has performed science-quality observations. The TEMPEST-D radiometer has similar or better performance to large satellites in terms of calibration accuracy, instrument noise, and calibration stability or precision. Chandrasekar et al. [8] and Radhakrishnan et al. [9] cross validated TEMPEST-D and RainCube CubeSat observations. This study showed that even though these two microwave instruments are heterogeneous, i.e., RainCube is an active radar and TEMPEST-D is a microwave

Manuscript received 7 April 2023; revised 18 May 2023 and 12 July 2023; accepted 28 July 2023. Date of publication 4 August 2023; date of current version 15 August 2023. This work was supported by the NASA Earth Venture Technology Demonstration Program under Grant NNX15AP56G, Grant 80NSSC20K1124, and Grant 80NSSC21K2073 to Colorado State University. *(Corresponding author: Chandrasekar Radhakrishnan.)*

Chandrasekar Radhakrishnan is with the The Cooperative Institute for Research in the Atmosphere, Colorado State University, Fort Collins, CO 80523 USA (e-mail: chandrasekar.radhakrishnan@colostate.edu).

V. Chandrasekar and Steven C. Reising are with the Department of Electrical and Computer Engineering, Colorado State University, Fort Collins, CO 80523 USA (e-mail: chandra@colostate.edu; steven.reising@colostate.edu).

Wesley Berg is with the Department of Atmospheric Science, Colorado State University, Fort Collins, CO 80523 USA (e-mail: wesley.berg@colostate.edu).

Shannon T. Brown is with the Jet Propulsion Laboratory, California Institute of Technology, Pasadena, CA 91109 USA (e-mail: shannon.t.brown@jpl.nasa.gov).

Digital Object Identifier 10.1109/JSTARS.2023.3302025

radiometer (a passive instrument), their observations are physically consistent. Radhakrishnan et al. [10] estimated surface rainfall from TEMPEST-D TB observations using a machine-learning approach based on an artificial neural network. They reported that the resulting rainfall matches the ground weather radar rainfall product in terms of location and intensity.

These studies demonstrated that TEMPEST-D is a highly successful mission. Nevertheless, TEMPEST-D observations need to be compared with those from traditional satellites. Berg et al. [7] validated TEMPEST-D observations through comparison with operational satellites only for clear sky cases and not for precipitating systems. The present study focuses on validating TEMPEST-D observations in comparison to traditional satellites over precipitating systems, as well as evaluating the impact of merging TEMPEST-D observations with those of traditional satellites. With the goal of continuing validation and use of TEMPEST-D data for atmospheric science, this study compares TEMPEST-D observations with well-calibrated GMI observations. GPM is a highly successful international satellite mission conducted by the National Aeronautics and Space Administration and the Japan Aerospace Exploration Agency. GMI measures PMW radiances from the Earth's surface and atmosphere in 13 channels. The rest of this article is organized as follows. Section II provides information on the TEMPEST-D mission and observations over severe storms. Section III gives the details of methodology followed in this study to cross compare the TEMPEST-D and GMI observations. Section IV discuss the results. Finally, Section V concludes this article.

II. TEMPEST-D CubeSat Mission

The TEMPEST-D CubeSat mission operated on orbit for nearly three years and observed more than 400 storms, including three consecutive hurricane seasons. TEMPEST is a 6U CubeSat mission concept to observe the evolution of cloud convective systems with high temporal resolution. The TEMPEST constellation mission concept comprises 6–8 identical 6U CubeSats deployed in the same orbital plane with approximately 5-minute spacing [11]. The TEMPEST-D ("D for demonstration") satellite is a 6U CubeSat launched as part of a resupply mission to the International Space Station (ISS) on May 21, 2018 and deployed from the ISS into orbit on July 13, 2018. Fig. 1 shows the TEMPEST-D CubeSat on orbit shortly after deployment. The TEMPEST-D radiometers measure at five millimeter-wave frequencies (87, 164, 174, 178, and 181 GHz) that provide detailed information on convection as well as the surrounding water vapor. Padmanabhan et al. [12] provided a detailed description of the instrument and prelaunch calibration. The TEMPEST-D mission performed continuous observations of the atmosphere for nearly three years. The radiometric performance of the TEMPEST-D instrument has been validated to be equivalent to on-orbit operational sensors on current-generation satellites, as shown by Berg et al. [7]. TEMPEST-D has demonstrated the necessary technology for the success of the TEMPEST constellation. TEMPEST-D TB imagery of tropical cyclones

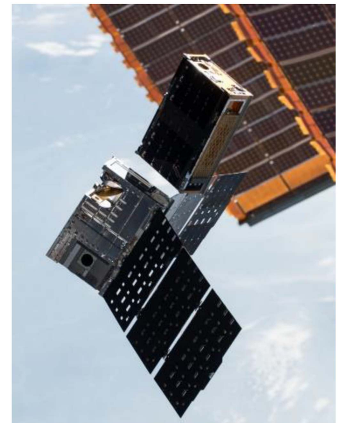

Fig. 1. Image of TEMPEST-D CubeSat just after deployment from the international space station.

observed over the world's oceans is shown in Figs. 2–5. The black dashed lines indicate the center of the TEMPEST-D swath. Specifically, Fig. 2 shows TEMPEST-D observations of hurricanes over the Atlantic Ocean. Similarly, Fig. 3 shows hurricanes observed by TEMPEST-D over the eastern Pacific Ocean. In addition, Fig. 4 shows tropical cyclone observations over the Indian Ocean, and Fig. 5 shows typhoons observed by TEMPEST-D over the Western Pacific Ocean. In terms of the life cycle of tropical cyclones, Fig. 2(a) shows Hurricane Florence in an intense phase, and Fig. 3(b) shows Hurricane Douglas in a low intensity phase over the open ocean. Fig. 4(c) shows Cyclone Nisarga making landfall, and Fig. 5(b) shows Typhoon Lekima near the coast of Taiwan. In summary, Figs. 2–5 provide evidence of the high quality and availability of TEMPEST-D observations to study various stages in the life cycle of tropical cyclones.

III. Methodology

This study uses the TEMPEST-D 164 GHz quasi-horizontal (QH) as well as GMI 166 GHz horizontal and vertical channel observations for cross comparison. Two methodologies are utilized for cross validation of TEMPEST-D and GMI TB observations. The first methodology is to quantitatively compare TEMPEST-D and GMI observations over precipitation systems over different parts of the Earth using a priori spatiotemporal constraints. The second cross-validation methodology is to quantitatively compare TEMPEST-D and GMI TB imagery over tropical cyclones.

A. Methodology for Comparison Over Precipitating Systems

Like many other microwave atmospheric sounders, TEMPEST-D is a cross-track scanning radiometer. On the other hand, GMI is a conically-scanning radiometer. The geometry of the different scan patterns of TEMPEST-D and GMI is shown in Fig. 6. The GMI views the scene at a constant Earth incidence angle (EIA) of 49.1°. The GMI pixel size for the 166 GHz channel is 13 km, which is constant over its scan. Since TEMPEST-D is cross-track scanning, the EIA

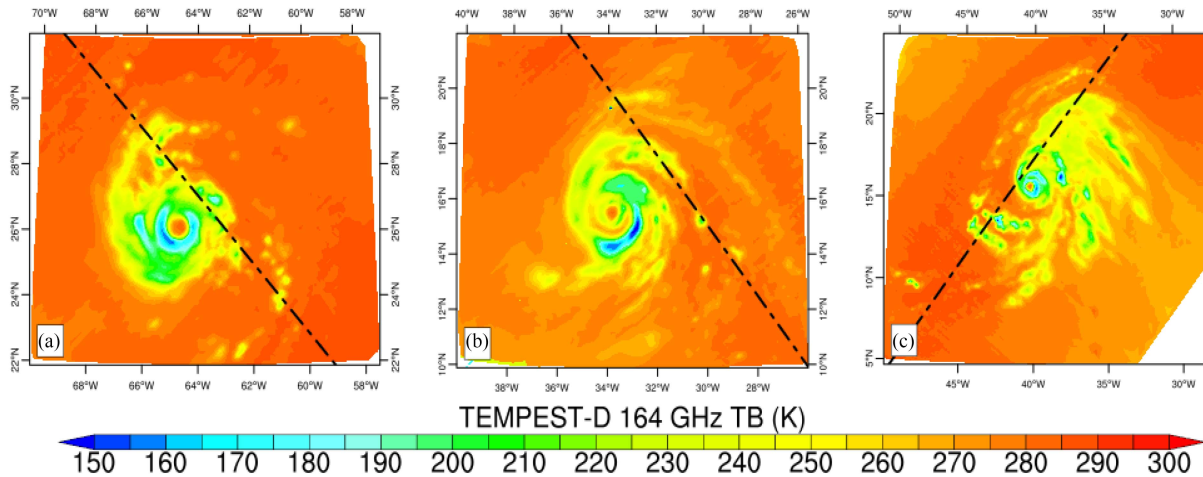

Fig. 2. TEMPEST-D observations over Atlantic ocean hurricanes. (a) Hurricane Florence on September 11, 2018 between 11:48 and 11:53 UTC. (b) Hurricane Isaac on September 11, 2018 between 10:18 and 10:23 UTC. (c) Hurricane Lorenzo on September 26, 2019 between 16:51 and 16:59 UTC.

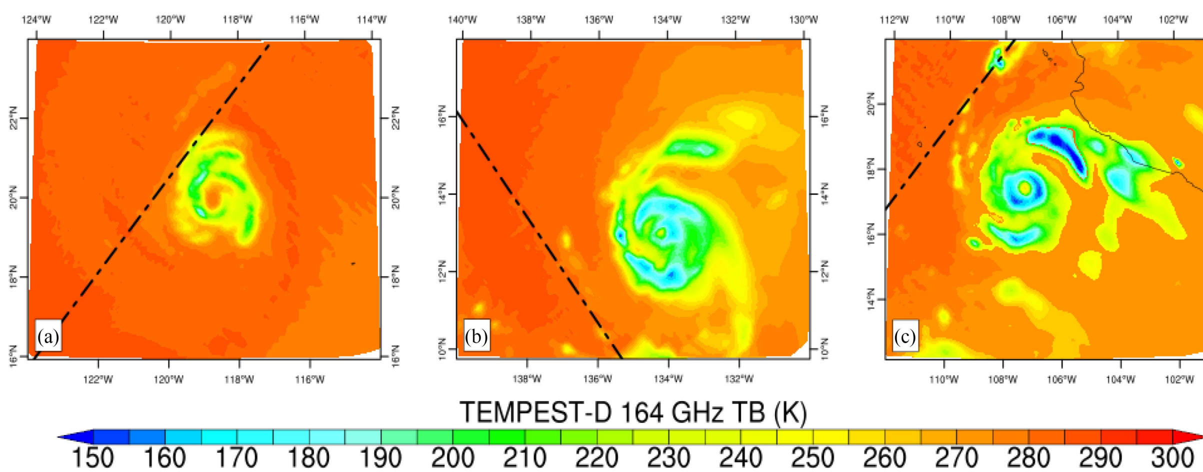

Fig. 3. TEMPEST-D observations over hurricanes in the Eastern Pacific ocean. (a) Hurricane Juliette on September 5, 2019 between 06:59 and 70:02 UTC. (b) Hurricane Douglas on July 23, 2020 between 09:03 and 09:06 UTC. (c) Hurricane Genevieve on August 18, 2020 between 10:27 and 10:33.

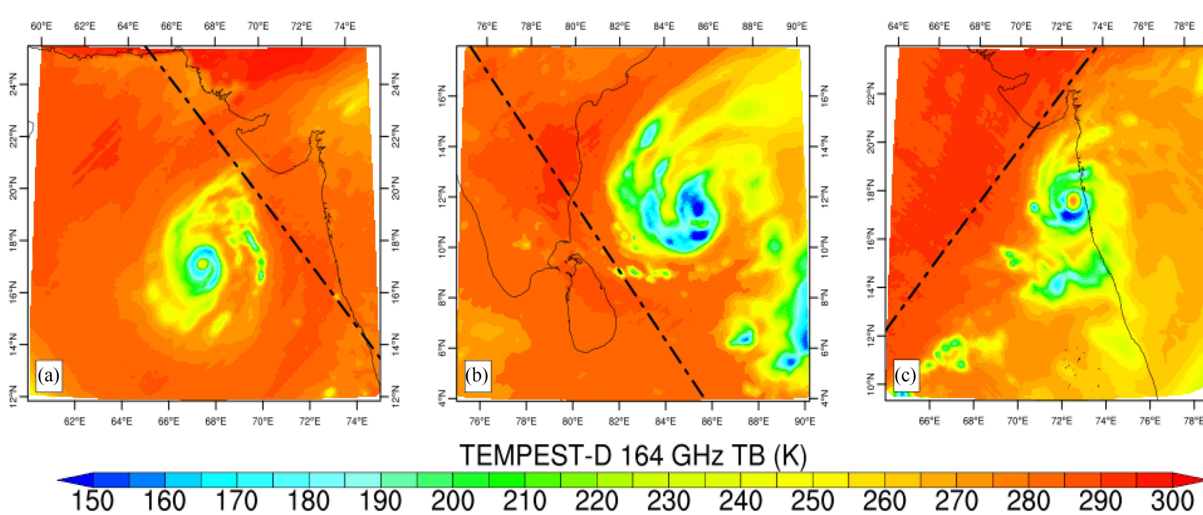

Fig. 4. TEMPEST-D observations over tropical cyclones in the Indian ocean. (a) Cyclone Kyarr on October 10, 2019 between 07:14 and 07:18 UTC. (b) Cyclone Amphan on May 16, 2020 between 21:43 and 21:49 UTC. (c) Cyclone Nisarga on June 3, 2020 between 05:09 and 05:15 UTC.

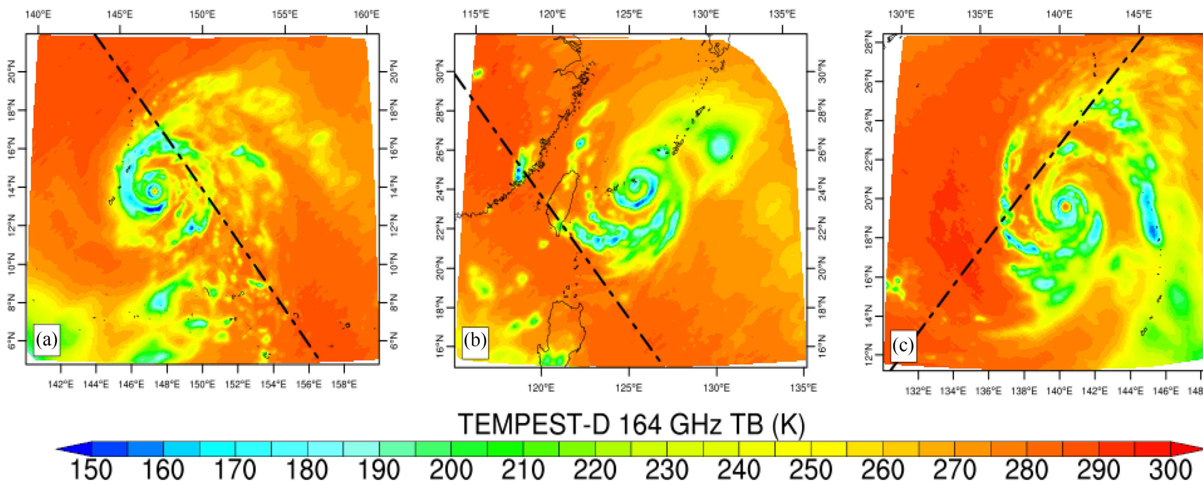

Fig. 5. TEMPEST-D Observations over typhoons in the Western Pacific ocean. (a) Typhoon Yutu on October 24, 2018 between 05:19 and 05:26 UTC. (b) Typhoon Lekima on August 08, 2019 between 11:37 and 11:43 UTC. (c) Typhoon Hagibis on October 09, 2019 between 00:16 and 00:23 UTC.

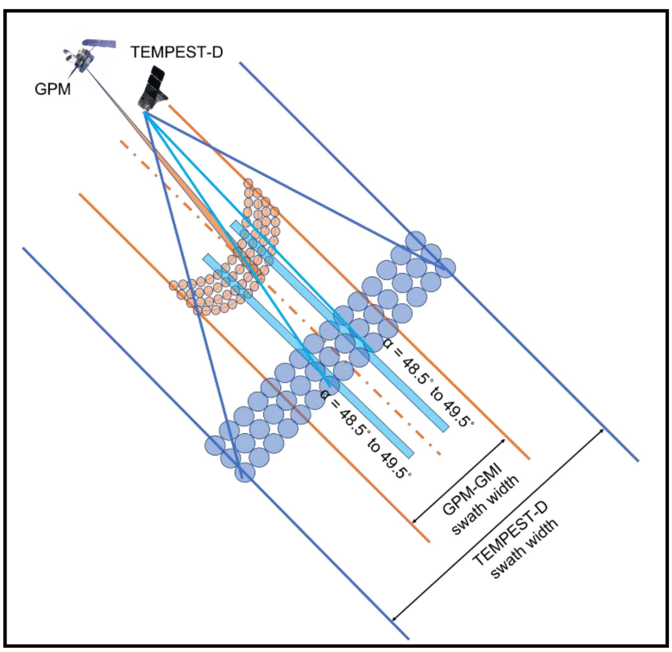

Fig. 6. Conceptual diagram of cross validation of TEMPEST-D and GMI observations.

changes during the scan, similar to the NOAA Advanced Technology Microwave Sounder [13]. The TEMPEST-D footprint size at nadir is 25 km for the 87 GHz channel and 12.5 km for the 164, 174, 178, and 181 GHz channels. The TEMPEST-D observations used in this study are from the 164 GHz QH channel. In contrast, GMI provides horizontally and vertically polarized observations at 166 GHz. Therefore, the cross-comparison procedure needs to take into account the scanning geometry, the spatiotemporal difference between these two instruments, and the polarization rotation of GMI measured TBs to QH polarization before applying the cross validation. The QH polarized TBs are estimated from the GMI measured TBs as [14]

$$\mathrm{TB}_{\mathrm{GMI(QH)}} = \mathrm{TB}_{\mathrm{GMI}(H)} \cos^2(\theta) + \mathrm{TB}_{\mathrm{GMI}(v)} \sin^2(\theta) \quad (1)$$

where $\mathrm{TB}_{\mathrm{GMI(QH)}}$ is the estimated GMI 166 GHz TB at QH polarization, $\mathrm{TB}_{\mathrm{GMI}(H)}$ is the GMI 166 GHz TB at horizontal polarization, $\mathrm{TB}_{\mathrm{GMI}(V)}$ is the GMI 166 GHz TB at vertical polarization, and θ is the TEMPEST-D EIA.

As an example, Fig. 7 shows a precipitation system that was simultaneously observed by both TEMPEST-D and GMI over the Great Australian Bight on November 18, 2018. The time difference between two observations was less than 1.5 min. The blue dashed lines in Fig. 7 indicate the portions of the TEMPEST-D cross-track scan at $\pm$ 49° EIA, and the black dashed lines indicate the nadir tracks of the respective satellite. The quasi-horizontally polarized TBs from GMI are calculated for the common observations between TEMPEST-D and GMI on the blue dashed lines. Fig. 8 shows a flowchart of the process for comparison of precipitation system observations using a priori spatiotemporal constraints. The method has six steps as follows.

1) In the first step, nadir intersections of TEMPEST-D and GMI observations were identified and filtered to keep only intersections with a time difference of less than 30 min.
2) From the set of all common observations of TEMPEST-D and GMI identified in Step 1, extract only those data with precipitating systems, i.e., those including TB values below 240 K.
3) Extract the TEMPEST-D observations with EIA values between 48.5° and 49.5°.
4) Extract GMI observations near the TEMPEST-D observations extracted in Step 3).
5) Calculate the QH TBs from GMI 166 GHz horizontal and vertical polarization channels by the polarization rotation algorithm described in [14].
6) Finally, the TEMPEST-D and GMI polarization-corrected observations are compared.

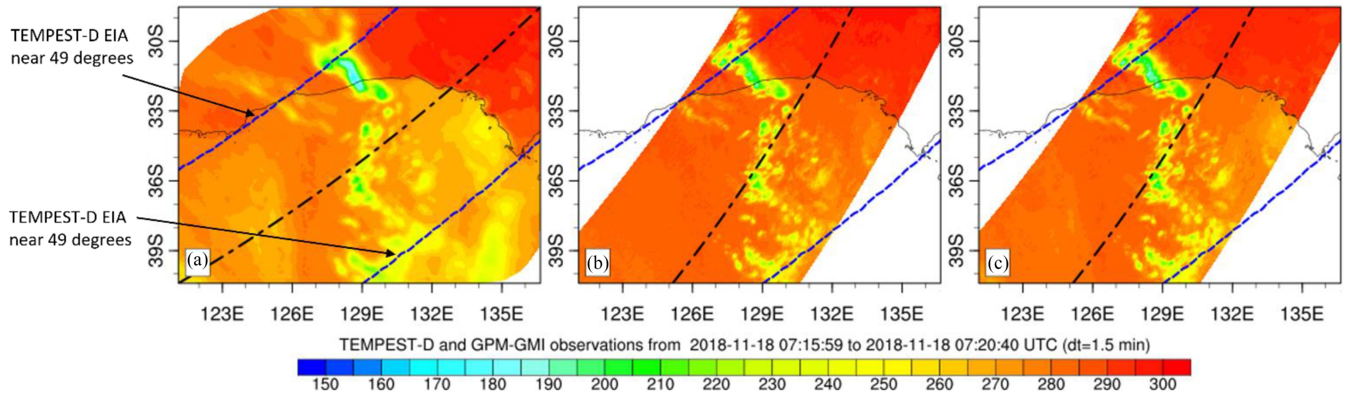

Fig. 7. TEMPEST-D and GMI observations over the Great Australian Bight on November 18, 2018. (a) TEMPEST-D TB (K) at 164 GHz. (b) GMI TB (K) at 166 (V) GHz. (c) GMI TB (K) at 166 (V) GHz.

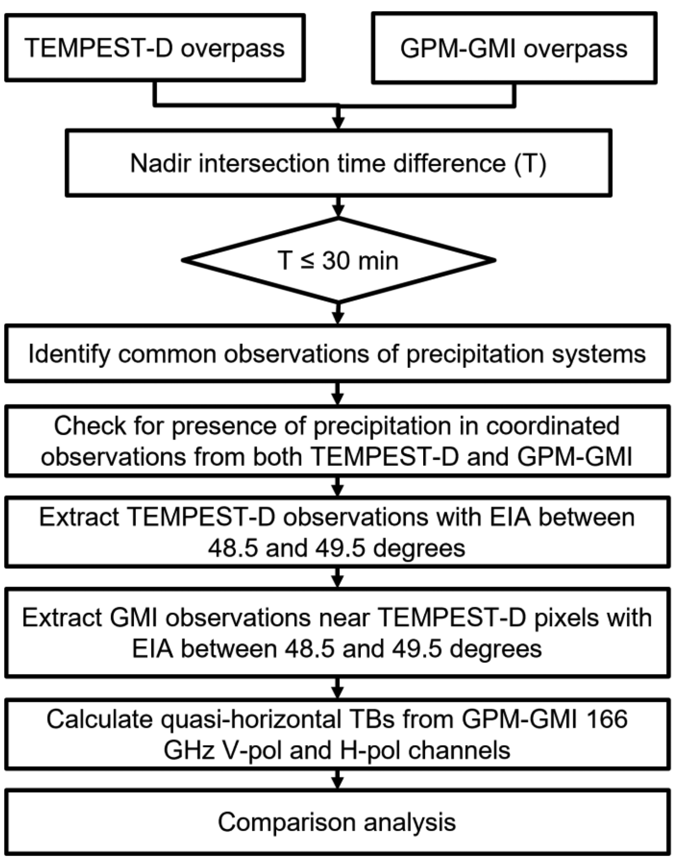

Fig. 8. Flowchart to select common observations for comparison.

B. Methodology for Comparison Over Tropical Cyclones

This method compares observations of TEMPEST-D and GMI over tropical cyclone systems observed by the two sensors within 1 h and 30 min. The objective of this comparison method is to estimate the correlation between two satellite instruments observing different portions of tropical cyclones. To do this, three lines at different scan angles have been drawn on the TEMPEST-D observed image of the tropical cyclone. Similarly, three lines are drawn on the GMI observed image. The center line is drawn through the eye of the tropical cyclone to analyze the characteristics of the storm eye structure from the two sensors' observations. The other two lines are offset from the center line by $\pm 0.5^{\circ}$ in latitude and longitude to compare the two instruments' observations over the tropical cyclones' rain bands. At the lines on the images, TEMPEST-D and GMI data have 26-km and 13-km footprint sizes, respectively. Then TB observations on those three lines were extracted from both TEMPEST-D and GMI hurricane observations. To match the footprint of GMI observations to that of TEMPEST-D observations, a two-point running average was performed on the GMI observations extracted from each line. To match the number of observations in GMI and TEMPEST-D, every other observation from GMI is chosen. The extracted datasets from TEMPEST-D and GMI have the same number of observations. These two sets of TB observations have a footprint size of 26 km and different times of observations over the same tropical cyclone system. Finally, the correlation coefficients (r) between TEMPEST-D and GMI TBs are calculated for each line.

IV. Results and Discussion

A. Comparison of Nearest Spatiotemporal Observations Over Precipitation Systems

This comparison study utilized all available TEMPEST-D observations between 2018 and 2021 and their corresponding GMI observations from all parts of the globe. After applying EIA range constraints of 48.5° to 49.5° to the TEMPEST-D data, as well as a priori spatial and temporal simultaneity constraints within 5 km and 30 min, 95 716 observation points were identified for use in the analysis. The QH polarization is calculated from GMI horizontal and vertical polarization channels for all 95 716 pixels and is compared with TEMPEST-D observations. This comparison between TEMPEST-D and GMI TB observations showed that the mean absolute difference between the two sets of TB observations is 2.9 K. The r value is 0.86 between TEMPEST-D and GMI. This analysis showed that

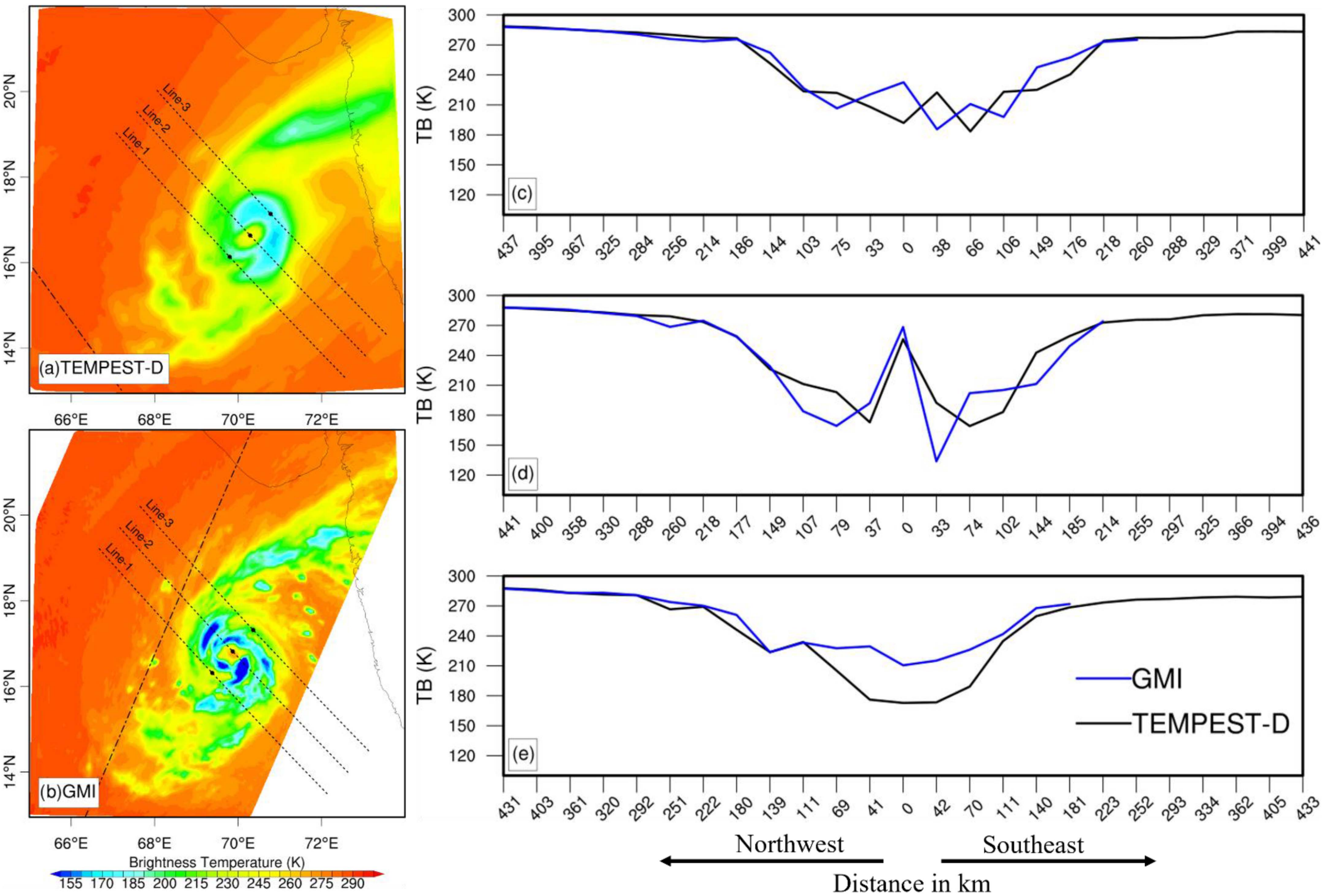

Fig. 9. (a) Super cyclone storm Kyarr observations from TEMPEST-D on October 26, 2019 from 08:12 to 08:15 UTC. (b) GMI observations from 09:05 to 09:08 UTC. (c) Comparison of TEMPEST-D and GMI TB observations at Lines 1 shown in (a) and (b). (d) Comparison of TEMPEST-D and GMI TB observations at Lines 2 shown in (a) and (b) over the eye of super cyclone storm Kyarr. (e) Comparison of TEMPEST-D and GMI TB observations at Lines 3 shown in (a) and (b).

TEMPEST-D performs similarly to GMI over precipitation systems. In contrast, Berg et al. [7] compared only clear-sky, oceanic observations from TEMPEST-D with those from multiple well-calibrated sensors observing at similar frequencies, including GMI and MHS on both NOAA and MetOp satellites. This is substantially different from the present study, which focuses on observations from precipitation systems over both ocean and land. In addition, Berg et al. [7] used the double-difference procedure, which largely removes from the analysis the impact of the instrument and viewing angle differences as well as errors in geophysical parameter data and radiative transfer models.

B. Quantitative Brightness Temperature Comparisons Over Tropical Cyclones

The first case for this comparison study is super cyclone storm Kyarr in the North Indian Ocean. It formed as a low-pressure system over the Arabian Sea near the Lakshadweep Islands on October 17, 2019, and intensified as a TC on October 25. TC Kyarr underwent rapid intensification and reached super cyclonic storm status on October 27, moved westward, and dissipated over the coast of Somalia on November 3, 2019. Kyarr was also the second strongest TC in the Arabian Sea and one of the most intense TCs in north Indian Ocean history. Fig. 9(a) shows TEMPEST-D observations of TC Kyarr on October 26, 2019 from 08:12 to 08:15 UTC, and Fig. 9(b) shows GMI observations on the same day from 09:05 to 09:08 UTC. The approximate time difference between these two observations was 52 min, and TEMPEST-D was leading GMI. The three lines shown in each of Fig. 9(a) and (b) are drawn starting at the black dots and extending to the northwest and the southeast. Fig. 9(c) shows the TEMPEST-D and GMI TB observations along Lines 1 shown in Fig. 9(a) and (b). Line 2 starts at the center of the eye of the storm as observed from TEMPEST-D and GMI, as can be seen in Fig. 9(d), where the eye of the storm is evident in the "W" shape signature. Fig. 9(e) shows the TEMPEST-D and GMI TB observations along Lines 3 shown in Fig. 9(a) and (b). Table I lists the values of r between TEMPEST-D and GMI TB observations of TC Kyarr for Lines 1–3, i.e., 0.87, 0.89, and 0.96, respectively.

The second case for this comparison study is Hurricane Sally, a very intense and slow-moving Atlantic hurricane, and the first to make landfall in the U.S. state of Alabama since 2004. Hurricane Sally developed from an area of disturbed weather

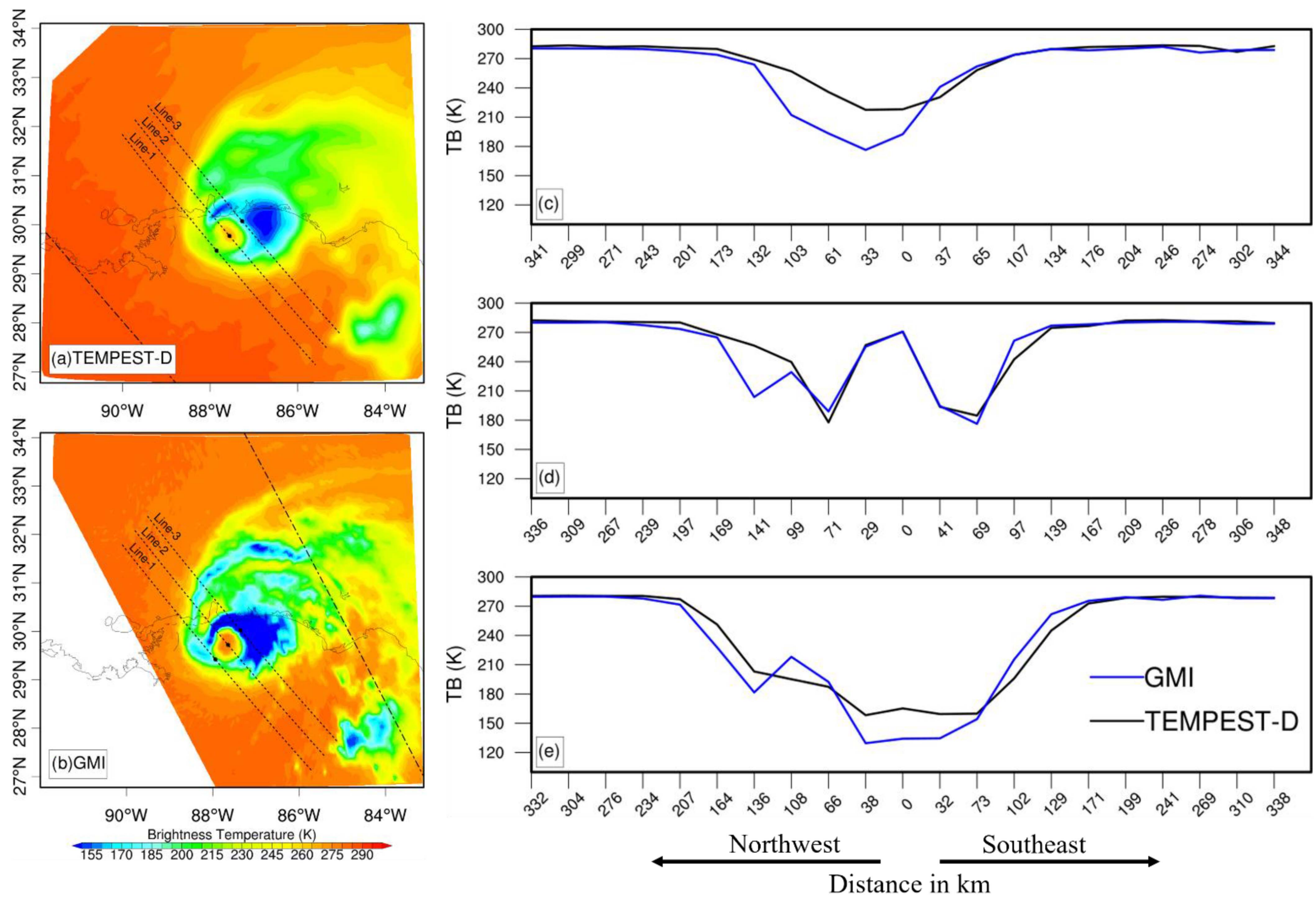

Fig. 10. (a) Hurricane Sally observations from TEMPEST-D on September 16, 2020 from 06:48 to 06:51 UTC. (b) GMI observations from 06:24 to 06:26 UTC. (c) Comparison of TEMPEST-D and GMI TB observations at Lines 1 shown in (a) and (b). (d) Comparison of TEMPEST-D and GMI TB observations at Lines 2 shown in (a) and (b) over the eye of the hurricane Sally. (e) Comparison of TEMPEST-D and GMI TB observations from Lines 3 shown in (a) and (b).

TABLE I
VALUES OF CORRELATION COEFFICIENT BETWEEN TEMPEST-D AND GMI OVER THE THREE LINES SHOWN IN FIGS. 9–11

Name	Line 1	Line 2	Line 3
Kyarr	0.87	0.89	0.96
Sally	0.93	0.93	0.96
Delta	0.94	0.73	0.80

near the Bahamas Islands on September 10, 2020. Sally became a Category 2 hurricane and made landfall on September 16, 2020 at 09:45 UTC near Gulf Shores, Alabama, with maximum sustained winds of 110 mi/h and a minimum central pressure of 965 hPa. Fig. 10(a) shows the TEMPEST-D observations over Hurricane Sally on September 16, 2020, from 06:48 to 06:51 UTC. Fig. 10(b) shows the GMI observations over Hurricane Sally, from 06:24 to 06:26 UTC. The average time difference between these two observations was 24 minutes; in this case, TEMPEST-D was lagging GMI. The hurricane's intensity and outer and inner core structure look similar in the two sets of observations. The three lines shown in Fig. 10(a) and (b) is drawn starting at the black dots and extending to the northwest and the southeast. Line 2 starts in the center of the eye of the hurricane in both images. Fig. 10(c) shows the TEMPEST-D and GMI TB observations along Lines 1 shown in Fig. 10(a) and (b). Similar to the previous case, the hurricane eye is evident in the "W" shape in Fig. 10(d). Fig. 10(e) shows the TEMPEST-D and GMI TB observations along Lines 3 shown in Fig. 10(a) and (b). In this case, the values of r between TEMPEST-D and GMI TB observations of Hurricane Sally are 0.93, 0.93, and 0.96 for Lines 1, 2 and 3, respectively, as listed in Table I. The TEMPEST-D and GMI TB observations from Lines 2 in Fig. 10(d) show that the TEMPEST-D and GMI-observed locations of the eye and structure of the hurricane are very similar to each other.

The third and final case for this comparison study is Hurricane Delta. Fig. 11(a) shows the Hurricane Delta observations from TEMPEST-D on October 7, 2020 from 12:59 to 13:02 UTC. Fig. 11(b) shows the GMI observations from 14:09 to 14:11 UTC. In this case, TEMPEST-D leads GMI by 1 h and 10 min. Features of Hurricane Delta look similar in the two sets of observations. However, GMI observations show more intense features than TEMPEST-D observations since the hurricane intensified between the TEMPEST-D and GMI observations. Fig. 11(a) and (b) shows the three lines starting at the black dots and extending to the northeast and the southwest. Fig. 11(c) and (e) shows the TEMPEST-D and GMI TB observations along

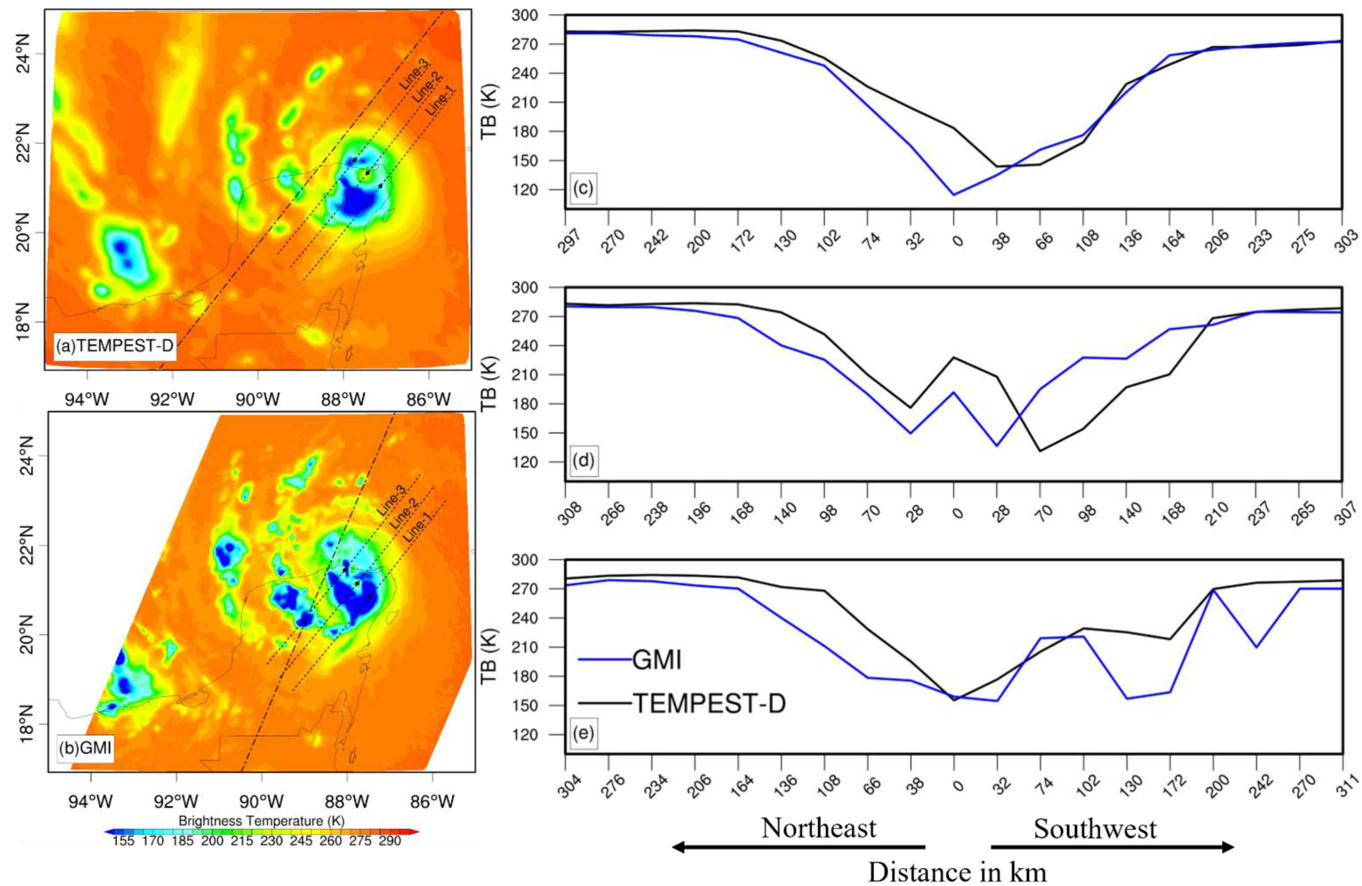

Fig. 11. (a) Hurricane Delta observations from TEMPEST-D on October 7, 2020 from 12:59 to 13:02 UTC. (b) GMI observations from 14:09 to 14:11 UTC. (c) Comparison of TEMPEST-D and GMI TB observations at Lines 1 shown in (a) and (b). (d) Comparison of TEMPEST-D and GMI TB observations at Lines 2 shown in (a) and (b) over the eye of the hurricane Delta. (e) Comparison of TEMPEST-D and GMI TB observations from Lines 3 shown in (a) and (b).

Lines 1 and 3, respectively. Similar to the previous two cases, in this case, Line 2 passes through the hurricane eye location, as can be seen in Fig. 11(d). The values of r between TEMPEST-D and GMI observations are 0.94, 0.73, and 0.80, for Lines 1, 2, and 3, respectively, as given in Table I. The results show that TEMPEST-D and GMI-observed locations of the eye of the hurricane are very similar, and the hurricane's structure also agrees well between the two sets of observations.

C. Merged TEMPEST-D and GMI Storm Track

The cross validation of TEMPEST-D and GMI observations over precipitating systems has demonstrated good agreement. This provides increased confidence in the ability to merge the two observations to improve tropical cyclones tracking. To test this hypothesis, this study used three cylones, i.e., Hurricane Dorian, Typhoon Hagibis, and Tropical Cyclone Kyarr. All available overpasses from TEMPEST-D and GMI within the period of storms were collected. This showed that due to their differing LEO orbits, the two instruments observed the storms at different times. The storm eye location was identified for all overpasses from TEMPEST-D and GMI observations. A storm track was drawn by combining the eye locations from the two instruments. Then the TEMPEST-D and GMI composite track was compared with the NOAA best track. In the first case, Hurricane Dorian, Fig. 12 shows the NOAA best track, GMI-only track, and TEMPEST-D-GMI combined track of Hurricane Dorian between August 28 and September 6, 2019. In the case of Hurricane Dorian, TEMPEST-D has nine observations, and GMI has seven observations. Fig. 12 clearly shows that the combined track is closer to the NOAA best track than the GMI-only track is. In addition, when TEMPEST-D observations are combined with those from GMI, the number of observations within the hurricane period has more than doubled in comparison to GMI-only observations. In this case, the combined track has 16 eye locations, whereas GMI has only 7 eye locations. In the second case, Typhoon Hagibis, Fig. 13 shows the NOAA best track, GMI alone, and TEMPEST-D and GMI combined track for Typhoon Hagibis for October 6–12, 2019. In this case, TEMPEST-D has eight observations, and GMI has four observations of Typhoon Hagibis. Fig. 13 clearly shows that TEMPEST-D provided additional observations between GMI observations and improved the fit of the combined track with the NOAA best track, compared with the GMI-only track. Considered together, TEMPEST-D and GMI have 12 observations of Typhoon Hagibis, three times greater than the number of GMI observations alone. In the third case, Tropical Cyclone Kyarr, Fig. 14 shows the NOAA best track, GMI-only track,

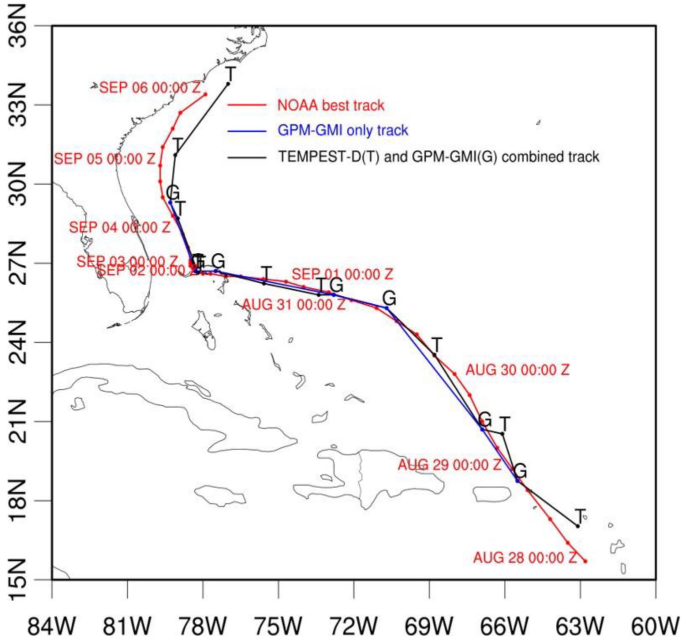

Fig. 12. Hurricane Dorian NOAA best track (red), GMI-only track (blue), and TEMPEST-D and GMI combined track (black) between August 28 and September 6, 2019.

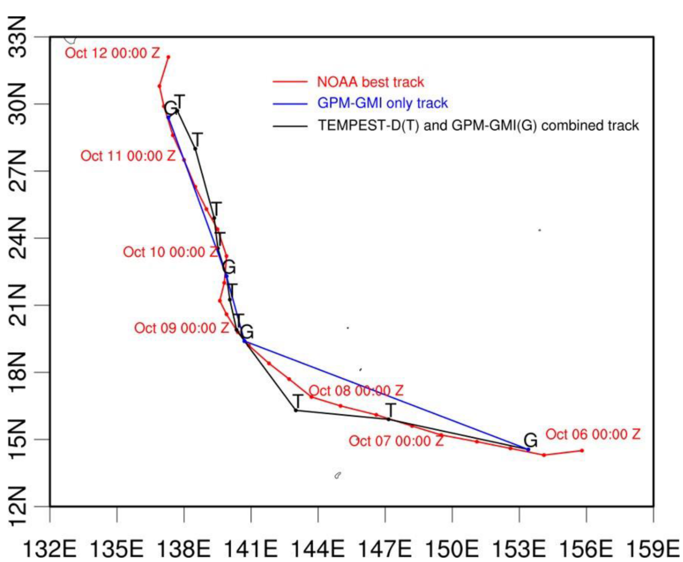

Fig. 13. Typhoon Hagibis NOAA best track (red), GMI-only track (blue), and TEMPEST-D and GMI combined track (black) for October 6–12, 2019.

and TEMPEST-D and GMI combined track of Tropical Cyclone Kyarr for October 25–30, 2019. TEMPEST-D and GMI each provide five observations of Tropical Cyclone Kyarr. The combined track is close to the best track, especially between October 26 and 27, 2019, during which no GMI observations are available, and TEMPEST-D observations provide the combined track, which is similar to the NOAA best track. As in the previous two cases, TEMPEST-D provided observations between the GMI observations and increased the total number of observations of Tropical Cyclone Kyarr. The results of the analysis

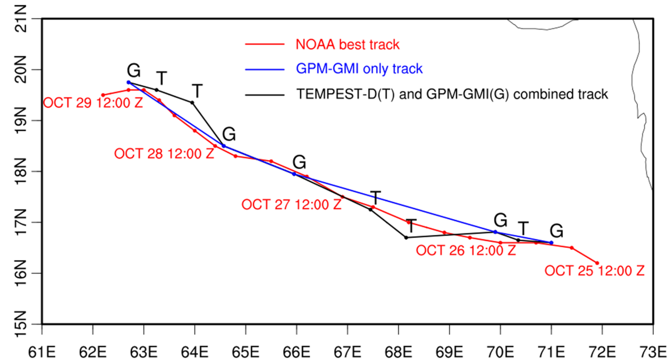

Fig. 14. Tropical Cyclone Kyarr NOAA best track (red), GMI-only track (blue), and TEMPEST-D and GMI combined track (black) for October 25–30, 2019.

of three tropical cyclones showed that TEMPEST-D provided additional observations between GMI observations and more than doubled the temporal frequency of TC observations. This storm track comparison study used observations of long-lived tropical cyclones over the ocean to demonstrate the impact of combined TEMPEST-D and GMI observations. This technique is also valid for storms over land, similar to over the ocean, since TEMPEST-D provides observations between GMI observations. This study demonstrated the impact of combined TEMPEST-D and GMI observations on storm track. Combining observations from these two satellite instruments will help to improve understanding of storm evolution, microphysics, and life cycles, as compared with observations from GMI or TEMPEST-D alone.

V. Conclusion

This study used two methodologies to cross-validate TEMPEST-D and GMI TB observations over precipitating systems. The first cross-validation methodology compared the observations over precipitating storms using a priori spatiotemporal constraints. The second methodology compared TEMPEST-D and GMI observations over tropical cyclone systems. For the first methodology, 95 716 observation points were identified after applying a priori spatiotemporal and EIA constraints. The results show that the two instruments' observations have similar TB distributions, and the mean absolute difference between them is 2.9 K, and the r value is 0.8. In the second cross-validation methodology, TEMPEST-D and GMI TB observations were compared over three tropical cyclones, Tropical Cyclone Kyarr, Hurricane Sally, and Hurricane Delta. TEMPEST-D and GMI observed these TCs at different times. The average r value between TEMPEST-D and GMI TBs for these three tropical cyclones was 0.9. The results of these two cross-validation analyses showed that TEMPEST-D observations are of similar quality to GMI observations over precipitating systems. The high correlation between the two instruments' observations provided increased confidence to merge the two sets of observations to improve tropical cyclone tracking. To this end, this study combined TEMPEST-D and GMI observations over three tropical cyclones to determine if the addition of TEMPEST-D to GMI observations improves the sampling frequency and track observation of TCs. For Hurricane Dorian, the addition of TEMPEST-D observations more doubles the temporal sampling frequency in comparison with GMI alone. For Typhoon Hagibis and Tropical Cyclone Kyarr, adding TEMPEST-D observations triples and doubles, respectively, the temporal sampling frequency from GMI alone.

This analysis of the three tropical cyclone storm cases shows that TEMPEST-D increases the temporal sampling frequency over TCs by approximately 2.5 times. The results of this study demonstrate that TEMPEST-D observations are of similar quality to those of traditional weather satellites in LEO over precipitation systems. In addition, the results show that TEMPEST-D observations can be merged with those of traditional satellites to increase the temporal frequency of weather observations from LEO on a global basis.

Acknowledgment

TEMPEST-D is a collaborative program with Caltech/NASA Jet Propulsion Laboratory and Blue Canyon Technologies. The authors would like to thank T. Gaier, S. Brown, S. Padmanabhan, and B. Lim of JPL for producing the TEMPEST-D radiometer instrument and providing calibrated and geolocated TBs. The authors would also like to thank P. Millar, G. Komar, B. Bauer, and S. Babu for their on-going support, encouragement, and program management.

References

[1] S. Ramanujam et al., "A new PCA-ANN algorithm for retrieval of rainfall structure in a precipitating atmosphere," *Int. J. Numer. Methods Heat Fluid Flow*, vol. 21, no. 8, pp. 1002–1025, 2011.

[2] S. Ramanujam, C. Radhakrishnan, D. Subramani, and B. Chakravarthy, "On the effect of non-raining parameters in retrieval of surface rain rate using TRMM PR and TMI measurements," *IEEE J. Sel. Topics Appl. Earth Observ. Remote Sens.*, vol. 5, no. 3, pp. 735–743, Jun. 2012.

[3] C. Balaji et al., "On the possibility of retrieving near-surface rain rate from the microwave sounder SAPHIR of the Megha-Tropiques mission," *Curr. Sci.*, vol. 106, no. 4, pp. 587–593, 2014.

[4] E. Kulu, *Nanosatellite and CubeSat Database*, Accessed: Oct. 26, 2022. [Online] Available: [Online]. Available: https://www.nanosats.eu/database

[5] Y. V. Goncharenko, W. Berg, S. C. Reising, F. Iturbide-Sanchez, and V. Chandrasekar, "Design and analysis of CubeSat microwave radiometer constellations to observe temporal variability of the atmosphere," *IEEE J. Sel. Topics Appl. Earth Observ. Remote Sens.*, vol. 14, pp. 11728–11736, 2021.

[6] R. M. Schulte et al., "A passive microwave retrieval algorithm with minimal view-angle bias: Application to the TEMPEST-D CubeSat mission," *J. Atmos. Ocean. Technol.*, vol. 37, no. 2, pp. 197–210, 2020.

[7] W. Berg et al., "Calibration and validation of the TEMPEST-D CubeSat radiometer," *IEEE Trans. Geosci. Remote Sens.*, vol. 59, no. 6, pp. 4904–4914, Jun. 2021.

[8] V. Chandrasekar et al., "Cross validation of TEMPEST-D and RainCube observations," in *Proc. IEEE Int. Geosci. Remote Sens. Symp.*, 2021, pp. 7892–7895.

[9] C. Radhakrishnan et al., "Cross validation of TEMPEST-D and RainCube observations over precipitation systems," *IEEE J. Sel. Topics Appl. Earth Observ. Remote Sens.*, vol. 15, pp. 7826–7838, 2022.

[10] C. Radhakrishnan, V. Chandrasekar, W. Berg, and S. C. Reising, "Rainfall estimation from TEMPEST-D CubeSat observations: A machine-learning approach," *IEEE J. Sel. Topics Appl. Earth Observ. Remote Sens.*, vol. 15, pp. 3626–3636, 2022.

[11] S. C. Reising et al., "An earth venture in-space technology demonstration mission for temporal experiment for storms and tropical systems (TEMPEST)," in *Proc. IEEE Int. Geosci. Remote Sens. Symp.*, 2018, pp. 6301–6303.

[12] S. Padmanabhan et al., "TEMPEST-D radiometer: Instrument description and prelaunch calibration," *IEEE Trans. Geosci. Remote Sens.*, vol. 59, no. 12, pp. 10213–10226, Dec. 2021.

[13] E. Kim, H. J. Lyu, K. Anderson, R. V. Leslie, and W. J. Blackwell, "S-NPP ATMS instrument prelaunch and on-orbit performance evaluation," *J. Geophysical Res., Atmos.*, vol. 119, no. 9, pp. 5653–5670, 2014.

[14] D. Draper, Q. Remund, D. Newell, and S. Krimchansky, "A comparison of GPM Microwave Imager (GMI) high frequency channel brightness temperatures to the advanced technology microwave sounder (ATMS)," in *Proc. IEEE Int. Geosci. Remote Sens. Symp.*, 2015, pp. 5146–5149, doi: 10.1109/IGARSS.2015.7326992.

Chandrasekar Radhakrishnan received the bachelor's degree from Anna University, Chennai, India, in 2006, and the Ph.D. degree from the Indian Institute of Technology Madras, Chennai, India, in 2013, both in mechanical engineering.

He was a Research Scientist with IBM India Research Laboratory, New Delhi, India. He is currently a Research Scientist with CIRA, Colorado State University, Fort Collins, CO, USA. His areas of interest are numerical weather prediction, data assimilation, satellite meteorology, radar-based nowcasting, and machine learning.

V. Chandrasekar (Fellow, IEEE) received the bachelor's degree from the Indian Institute of Technology Kharagpur, Kharagpur, India, in 1981, and the Ph.D. degree from Colorado State University (CSU), Fort Collins, CO, USA, in 1986, both in electrical engineering.

He has been the Director of the Research Experiences for Undergraduate Program for more than 25 years, where he is involved in promoting research in the undergraduate curriculum. He is currently a University Distinguished Professor with CSU. He is also the Research Director of the National Science Foundation Engineering Research Center for Collaborative Adaptive Sensing of the Atmosphere. He has been actively involved in the research and development of weather radar systems for more than 30 years. He has played a key role in developing the CSU-CHILL National Radar Facility as one of the most advanced meteorological radar systems available for research and continues to work actively with the CSU-CHILL radar, supporting its research and education mission. He has authored two textbooks and five general books and more than 250 peer-reviewed journal articles. He is an avid experimentalist conducting special experiments to collect in situ observations to verify the new techniques and technologies.

Dr. Chandrasekar is a Fellow of the American Meteorological Society, the American Geophysical Union, the International Union of Radio Science, and the National Oceanic and Atmospheric Administration (NOAA) Cooperative Institute for Research in the Atmosphere. He was a recipient of numerous awards, including Knighted by the Government of Finland, the NASA Technical Contribution Award, NASA Group Achievement Award, the NASA Robert H. Goddard Exceptional Achievement Award, the Outstanding Advisor Award, the IEEE GRSS Education Award, the NOAA/NWS Directors Medal of Excellence, and the IEEE GRSS Distinguished Achievement Award. He has served as the General Chair for the IEEE International Geoscience and Remote Sensing Symposium (IGARSS 2006).

Steven C. Reising (Senior Member, IEEE) received the B.S.E.E. (*magna cum laude*) and M.S.E.E. degrees in electrical engineering from Washington University, St. Louis, MO, USA, in 1989 and 1991, respectively, and the Ph.D. degree in electrical engineering from Stanford University, Stanford, CA, USA, in 1998.

He served as an Assistant Professor of electrical and computer engineering with the University of Massachusetts Amherst, Amherst, MA, USA, where he received tenure. He served as a Summer Faculty Fellow for three summers with the Remote Sensing Division, Naval Research Laboratory, Washington, DC, USA. In 2004, he joined Colorado State University, Fort Collins, CO, USA, where he served as an Associate Professor from August 2004 to June 2011, and has been a Full Professor of electrical and computer engineering since July 2011. He has served as a Principal Faculty Advisor for 18 M.S./Ph.D. students, who have completed their degrees and are currently employed as professors, engineers, and researchers in universities, industry, and government laboratories. He has been a Principal Investigator of 22 grants and contracts from NASA, NOAA, the National Science Foundation (NSF), the Office of Naval Research, National Polar-Orbiting Operational Environmental Satellite System Integrated Program Office, European Space Agency, Ball Aerospace, and FIRST RF. His research interests include a broad range of remote sensing disciplines, including microwave remote sensing of the Earth's atmosphere and oceans from airborne platforms, small satellites, and CubeSats; the design and development of radiometer systems from microwave to submillimeter-wave and THz frequencies (18– 850 GHz); Lidar systems for sensing temperature and winds in the middle and upper atmosphere; and lightning-ionosphere interactions and atmospheric electrodynamics.

Dr. Reising was a recipient of the NSF CAREER Award (in the areas of physical and mesoscale dynamic meteorology from 2003 to 2008), the Office of Naval Research Young Investigator Program Award for passive microwave remote sensing of the oceans from 2000 to 2003, the 2023 Terahertz Science and Technology Best Paper Award from the IEEE Microwave Theory and Technology Society, and the 2023 Harry Rosenberg Distinguished Service Award from Colorado State University. He has been serving as the Secretary of the IEEE Geoscience and Remote Sensing Society since 2021 (GRSS). He previously served as the Chair of the Ad-hoc Committee for Intersocietal Relations (2019–2020) and as an elected Administrative Committee (AdCom) Member of the IEEE GRSS from 2003 to 2020. He also previously served as an elected AdCom Member of the IEEE Microwave Theory and Techniques Society (MTT-S) from 2014 to 2019. He served the IEEE as MTT-S Inter-Society Committee Chair from 2015 to 2018, GRSS Vice President of Information Resources from 2011 to 2018, and the GRSS Vice President of Technical Activities from 2008 to 2010. He was a founding member of the *IEEE Geoscience and Remote Sensing Letters* Editorial Board and served as an Associate Editor from 2004 to 2013. He is a Guest Editor for three Special Issues and one Special Section of the IEEE TRANSACTIONS ON GEOSCIENCE AND REMOTE SENSING. He served as the Immediate Past Chair of the U.S. National Committee of the International Union of Radio Science (USNC-URSI) from 2015 to 2017, the Chair from 2012 to 2014, and the Secretary from 2009 to 2011, of all ten URSI Commissions. He is a member of URSI Commissions F, G, and H, the American Meteorological Society, the American Geophysical Union, the American Association for the Advancement of Science, Tau Beta Pi, and Eta Kappa Nu.

Wesley Berg received the B.S., M.S., and Ph.D. degrees in aerospace engineering from the University of Colorado, Boulder, CO, USA, in 1988, 1989, and 1993, respectively.

He worked with the Cooperative Institute for Research in Environmental Science, NOAA's Environmental Research Laboratories, Boulder, CO, USA. He is a Senior Research Scientist with the Department of Atmospheric Science, Colorado State University, Fort Collins, CO, USA. His research interests include satellite remote sensing of precipitation and other hydrologic parameters with a focus on instrument calibration and the development and analysis of satellite retrievals for long-term climate applications.

Shannon T. Brown (Senior Member, IEEE) received the B.S. degree in meteorology from Pennsylvania State University, State College, PA, USA, in 2001, and the M.S. degree in atmospheric science and the Ph.D. degree in geoscience and remote sensing from the University of Michigan, Ann Arbor, MI, USA, in 2003 and 2005, respectively.

He joined the Microwave Advanced Systems Section, Jet Propulsion Laboratory (JPL), Pasadena, CA, USA, in 2005, as a member. He is a Principal Technologist with NASA JPL. He has been involved in the space-borne Topex, Jason-1, 2, and 3 Microwave Radiometers, and the WindSat Polarimetric Radiometer. He is a Principal Investigator of the Compact Ocean Wind Vector Radiometer being developed for the U.S. Air Force and an Instrument Scientist for the NASA Juno Microwave Radiometer on the Juno New Frontiers mission to Jupiter. He is a member of the Ocean Surface Topography Science Team, the Ocean Salinity Science Team, the SMAP Science Team, and the Juno Science Team. His research interests include microwave radiometer system development, calibration, geophysical algorithm development for both passive and active sensors, extraction of climate data records, and radiometer science.

Dr. Brown was a recipient of the NASA Exceptional Achievement Medal in 2009, the JPL Lew Allen Award in 2010, eight NASA group achievement awards, and the NASA Space Act Award in 2012.